


Communication

Optical Design of an Integrated Paschen–Runge Spectrometer by Using a Multigrating Structure

Guo Xia ^{1,2,3,*} , Long Zhang ^{1,2,3}, Zhiwei Feng ^{1,2,3}, Wenjie Shi ^{1,2,3}, Lin Gao ^{1,2,3} and Yanduo Li ^{1,2,3}

¹ Key Laboratory of Special Display Technology of the Ministry of Education, National Engineering Laboratory of Special Display Technology, National Key Laboratory of Advanced Display Technology, Academy of Photoelectric Technology, Hefei University of Technology, Hefei 230009, China

² School of Instrument Science and Opto-Electronics Engineering, Hefei University of Technology, Hefei 230009, China

³ Anhui Province Key Laboratory of Measuring Theory and Precision Instrument, Hefei University of Technology, Hefei 230009, China

* Correspondence: xiaguo@hfut.edu.cn

Abstract: An integrated direct-reading spectrometer scheme using seven concave gratings is proposed. At present, the optical design simulation has been completed, and the subsequent physical design may be carried out according to the simulation results. Ray-tracing software (Zemax) is used to divide the spectrum on the grating into seven bands, and an area array detector is used to receive the spectral signals simultaneously, which reduces the volume of the spectrometer and improves the spectral consistency. Using this method, a spectrometer covering 230–440 nm is designed, and the spectral resolution of the center wavelength corresponding to the seven grating windows of 230–260 nm, 260–290 nm, 290–320 nm, 320–350 nm, 350–380 nm, 380–410 nm, and 410–440 nm can reach 0.0974 nm, 0.0652 nm, 0.0361 nm, 0.0157 nm, 0.0838 nm, 0.0872 nm, and 0.1471 nm.

Keywords: Paschen–Runge spectrometer; optical design; multigrating



Citation: Xia, G.; Zhang, L.; Feng, Z.; Shi, W.; Gao, L.; Li, Y. Optical Design of an Integrated Paschen–Runge Spectrometer by Using a Multigrating Structure. *Photonics* **2022**, *9*, 920. <https://doi.org/10.3390/photonics9120920>

Received: 28 October 2022

Accepted: 26 November 2022

Published: 29 November 2022

Publisher's Note: MDPI stays neutral with regard to jurisdictional claims in published maps and institutional affiliations.



Copyright: © 2022 by the authors. Licensee MDPI, Basel, Switzerland. This article is an open access article distributed under the terms and conditions of the Creative Commons Attribution (CC BY) license (<https://creativecommons.org/licenses/by/4.0/>).

1. Introduction

Direct-reading spectrometers are widely used in modern scientific research and industrial production, playing an important role in material identification. With the advancement of the industry and changes in application scenarios, new requirements have been placed on the spectrometer. Reducing the size and improving integration have become the main development directions of the direct-reading spectrometer.

The direct-reading spectrometer is usually used for spectral analysis to detect different substances. In the 1850s, Kirchhoff and Bunsen designed and manufactured a relatively complete set of spectroscopic devices to research the characteristic spectra of different metal substances, which was the first practical spectrometer in the world [1]. By the 1880s, Henry A. Rowland had invented the concave grating, which has self-focusing characteristics and requires no additional collimating or focusing elements [2]. Then, in the 1940s, the first direct-reading spectrometer was developed and has been deeply researched and applied in many directions [3]. The traditional direct-reading spectrometer usually adopts the Paschen–Runge structure; the main components are concave grating with large curvature and a large amount of groove density, and multiple detectors are distributed on the Rowland circle [4–6]. In order to achieve high-resolution and wide waveband detection, long focal lengths and multiple linear detectors are usually used, resulting in a larger volume of the direct-reading spectrometer, which is inconvenient for on-site detection. However, it is difficult to achieve a wide-working waveband, high resolution, and high speed simultaneously in a small-volume spectrometer [7,8]. A possible solution to reduce the volume is using an adjustable mechanical structure; however, it is hard to quickly collect

multiple sets of spectral data during spectrum acquisition, and it is difficult to control the accuracy during the adjustment process and the stability during long-term use [9,10].

In the Czerny–Turner optical structure, researchers have proposed the idea of folding optical paths with integrated gratings. For example, Zhang et al. proposed the use of a five-grating integrated design and optimized the spectrometer in the wavelength range of 200–1000 nm [11]. Jiang et al. designed a high-resolution spectrometer with a wavelength range of 170–600 nm using 19 integrated gratings [12]. Tu et al. designed a coma-free ultrahigh-resolution spectrometer using 44 subgratings [13]. To best of our knowledge, no spectrometer with an integrated grating structure is used in the Paschen–Runge structure optical system.

With the rapid development of large-size area array detectors in recent years, an improved integrated grating spectrometer structure is proposed in this study. The structure adopts multiple concave subgratings and an area array detector. This design scheme reduces the volume of the traditional Paschen–Runge structure and facilitates on-site detection. At the same time, using an area array detector realizes the simultaneous acquisition of the spectrum and improves the consistency of the spectrum. The key parameters of area array detector imaging can be controlled by the angle of each subgrating on the meridional and sagittal planes. The optical system design and simulation analysis results are presented below.

2. Traditional Paschen–Runge Spectrometer

In optical systems using gratings as dispersive elements, when the light is incident on the grating at an angle α and then diffracted at an angle θ , the incident angle and the diffraction angle satisfy the grating equation:

$$d(\sin \alpha \pm \sin \theta) = m\lambda \quad (1)$$

where d is the grating constant, describing the distance between two adjacent grooves on the grating; and m is the diffraction order. In this design, the incident light and the diffracted light are on the same side of the grating normal, so the sign is positive; otherwise, the sign is negative. The entire wavelength range adopts first-order diffraction ($m = 1$), and Equation (1) can be rewritten as:

$$\sin \theta = \frac{\lambda}{d} - \sin \alpha \quad (2)$$

When the grating constant d and the incident angle α are determined, the diffracted spectral lines will be distributed in a wavelength window corresponding to the diffraction angles ranging from θ_1 to θ_2 , at this time:

$$\Delta \sin \theta = \sin \theta_2 - \sin \theta_1 = (\lambda_2 - \lambda_1)/d = \frac{\Delta \lambda}{d}, \quad (3)$$

As shown in Figure 1, the Paschen–Runge structure direct-reading spectrometer is mainly composed of a slit, a lens, a concave grating, and multiple line array detectors, all of which are located on the Rowland circle. It can be seen that the grating has a certain angle on the meridian plane, which reduces astigmatism in the wavelength range of 200–450 nm.

To precisely detect more element species (including some trace elements), the system is required to have a high spectral resolution, usually with a focal length of more than 500 mm and a grating of more than 2400 g/mm. In addition, the image plane of the optical system is located on the Rowland circle, and it is necessary to distribute enough detectors on the image plane to ensure the spectral resolution capability of the whole waveband. Therefore, these optics require high positioning accuracy, and the system requires high mechanical and thermal stability. On the other hand, the characteristic spectrum of some elements is located in the ultraviolet waveband, or even in the vacuum ultraviolet band (UVD). Since common detectors have a low spectral response to the ultraviolet band, the energy cannot

meet the requirements, and the surface of the detector that accepts this waveband needs to be coated with an ultraviolet enhancement film. To improve the spectral response of this waveband, the entire optical chamber needs to be kept in a vacuum state or continuously flushed with inert gas during use to prevent the vacuum ultraviolet waveband from being absorbed by oxygen.

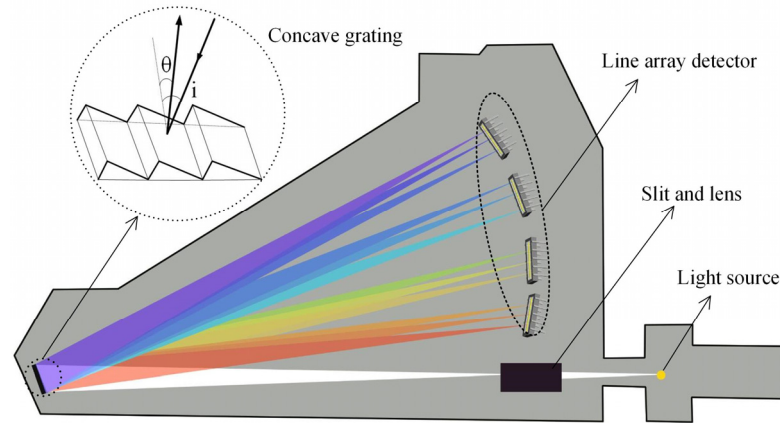


Figure 1. Traditional Paschen–Runge structure direct-reading spectrometer schematic.

3. Improved Integrated Paschen–Runge Spectrometer

The focus of this paper is the integration of grating, aiming to reduce the volume and size, ignoring the lens, mainly for the optical path model starting from the slit. As shown in Figure 2, the improved integrated direct-reading spectrometer designed is mainly composed of a slit, seven concave gratings, and an area array detector in this study. The optical path of the entire system is folded seven times on the sagittal plane, and a large-size area array detector is used to collect spectral information simultaneously, which improves the consistency of the spectrum. In comprehensive consideration of the wavelength range, size, and resolution of the spectrometer system, we choose seven concave subgratings and divide the wavelength range into seven groups. The central wavelengths of these subwavelength windows are 245 nm (230–260 nm), 275 nm (260–290 nm), 305 nm (290–320 nm), 335 nm (320–350 nm), 365 nm (350–380 nm), 395 nm (380–410 nm), and 425 nm (410–440 nm).

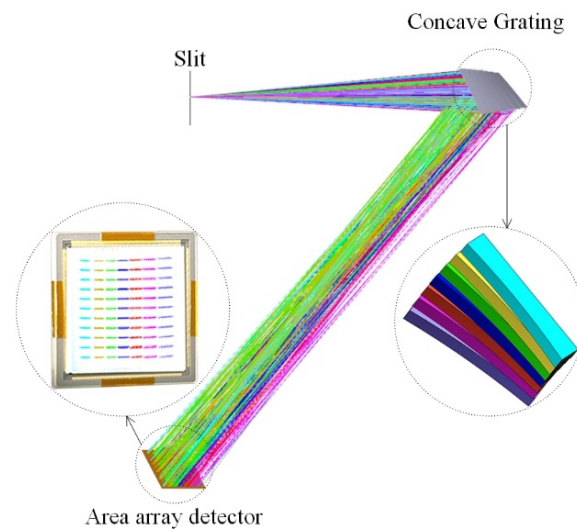
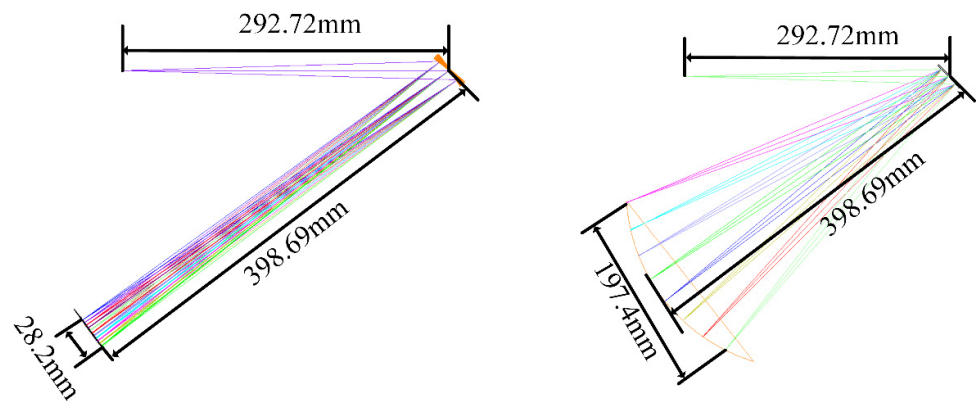


Figure 2. Structure of an integrated Paschen–Runge spectrometer.

According to the optical simulation results, the spot spacing of the edge grating among the seven gratings and the spot spacing corresponding to the upper edge wavelength of the same grating is about 29.8 mm × 32.3 mm. Secondly, the detector with a strong spectral response in the required band should be selected as far as possible, and the number of pixels of the detector should be as many as possible to meet the resolution requirements.

The pixel specification of the back-illuminated area array detector (QHY4040PRO-BSI [14]) is 4096 × 4096, the pixel size is 9 × 9 μm, and its effective imaging area is 36.9 × 36.9 mm. The first-order spectral resolving power of the concave grating can be given by $R = \lambda/\Delta\lambda = N$, where N is the total number of grooves on the grating. For a typical concave grating with a groove density of 2400 g/mm and a useful width of 35 mm, $R = 42,000$, the ideal wavelength resolution is about $\Delta\lambda = 0.004$ nm at $\lambda = 335$ nm.

In the traditional Paschen–Runge spectrometer described in Figure 1, multiple linear detectors are used because of the long rear focal length and wide image plane distribution on the entire Rowland circle, which is also the main reason for the large size of the traditional direct-reading spectrometer. In this paper, multiple gratings are integrated and distributed on the sagittal plane. By adjusting the angle of each grating, all the spectra can be received by a planar array detector, thus reducing the volume and improving. When the front focal length and rear focal length remain unchanged, the size of the image plane is reduced from 197.4 mm × 28 mm to 29.8 mm × 32.3 mm, as shown in Figure 3.



Improved Paschen - Runge optical system Traditional Paschen - Runge optical system

Figure 3. Size comparison of improved and traditional Paschen–Runge structured optical systems.

It can be seen in Figure 2, that the angles of the seven gratings on the meridional plane and the sagittal plane are different. Each grating has a different angle on the meridian plane so that the center wavelength of the corresponding band of each grating can be irradiated in the middle of the grating to avoid excessive off-axis aberration introduced by the edge wavelength. The tilt angle, curvature, and focal length of the central grating on the meridional plane are obtained according to the traditional Paschen–Runge structural parameter calculation method. According to Equations (1) and (3), the inclination angle of the grating on the meridian plane is calculated and adjusted carefully to make the sum of the incident angle and diffraction angle of the light before and after passing through the grating the same. This ensures that the diffraction length corresponding to each grating window remains the same on the premise of not exceeding the detector length. Since the detector receives the diffraction spectra of seven gratings at the same time, even if the width of each grating is set to 5 mm under the premise of ensuring the luminous flux, its spectral width still exceeds the width of the selected detector. At the same time, the angle of the grating on the sagittal plane has a linear relationship with the spectral width. By carefully adjusting the tilt angle of the grating on the sagittal plane, the spectral width can be limited to the size of the detector.

This optical design is simulated and optimized by ray-tracing software (Zemax). All the parameters are presented in Table 1.

Table 1. Main parameters of the optical structure.

Wavelength of Window $\Delta\lambda$	Distance from the Slit to the Grating f_1	Radius of Curvature of the Grating R_n	Angle of Incidence i_n	Angle on the Sagittal Plane β_n	Distance from the Grating to the Detector f_2
230–260 nm	292.5 mm	381.99 mm	36.2°	−1.45°	398.69 mm
260–290 nm		387.74 mm	38.5°	−1.05°	
290–320 nm		394.30 mm	40.85°	−0.55°	
320–350 nm		401.56 mm	43.2°	0°	
350–380 nm		410.13 mm	45.7°	0.55°	
380–410 nm		419.37 mm	48.12°	1.05°	
410–440 nm		430.03 mm	50.7°	1.45°	

As shown in Figure 4, the typical Paschen–Runge structure is retained on the meridian plane. The central grating, slit, and detector are still located on the Rowland circle, and the system optical path is integrated by using multiple concave gratings on the sagittal plane.

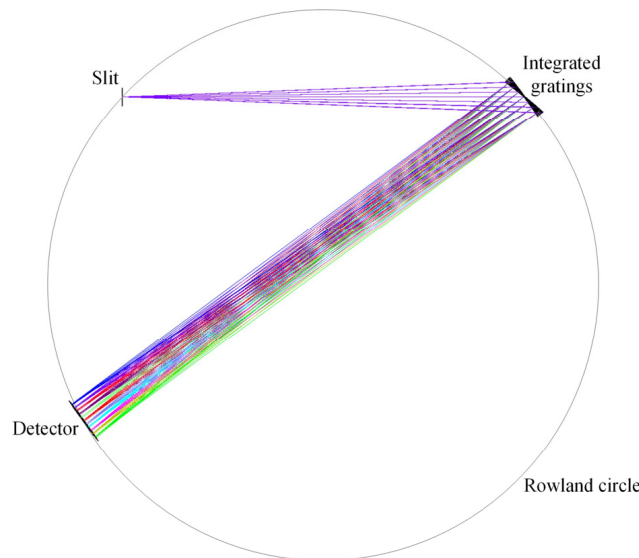


Figure 4. The layout of the integrated spectrometer was simulated. Slit, central grating, and detector on Rowland circle.

In the design of the Paschen–Runge spectrometer, the use of concave gratings made it unnecessary to use collimators and focusing mirrors. The main aberrations are caused by the off-axis angle of the concave grating, where the resolution is affected by the spherical and meridional coma aberrations, and the energy is affected by the image dispersion and sagittal aberrations. In the actual system, the verticality of the slit mounting, the machining accuracy, and the number of image elements of the detector also need to be considered, all of which have an impact on the optical performance of the system.

It is most common to evaluate an optical system’s performance according to the spot size, but in this integrated system, it is not intuitive for the method to directly observe the spot size. As shown in Figure 5, the Y-spot size data of each grating window interval of 3 nm is taken to make a circle with its spot radius. To evaluate the overall image quality, the spot size of the wavelength corresponding to all the grating windows is displayed intuitively [15].

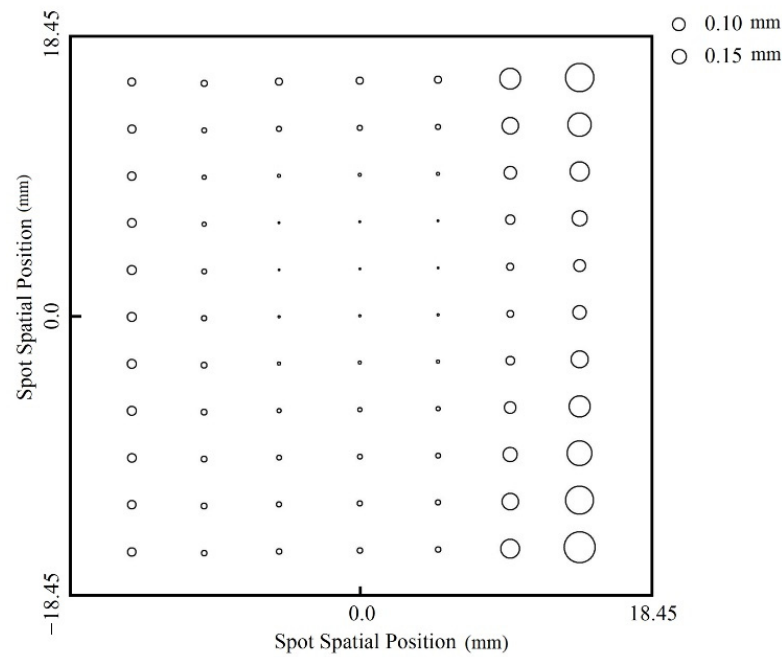


Figure 5. Y-spot radius at the position of the detector.

As shown in Figure 5, the Y-spot radius corresponding to the wavelength window of the central grating is the smallest, and the closer to the edge grating, the larger the spot size. For a single grating wavelength window, the center wavelength spot radius is the smallest, and the closer to the edge wavelength, the larger the spot radius, which is in line with the actual situation.

The spectral resolution is also an important parameter index for evaluating the spectrometer system, which is defined as the spectral bandwidth corresponding to one pixel in the detector. The wavelength distribution corresponding to each pixel can be obtained by convolution of the line spread function (LSF) of each pixel and a rectangular function with a pixel width of 10 μm, and the LSF can be obtained by the ray-tracing software. The distance along the pixel is convolved and then the corresponding convolution concerning wavelength is obtained, taking into account the grating dispersion [16]. The width of the slit is also one of the important factors affecting the resolution. The obtained result is convolved with the slit function of 10 μm, and its expression is defined as [17]:

$$f(\lambda) = f_S(x_s) \otimes f_{LSF}(\lambda) \otimes f_D(x_d) \tag{4}$$

where \otimes represents convolution; $f(\lambda)$ is the spectral line data corresponding to the wavelength; $f_S(x_s)$ and $f_D(x_d)$ represent the effect functions of the slit and detector, respectively, defining the influence of the slit module and detector module on the final detection spectrum; and $f_{LSF}(\lambda)$ represents the line spread function.

The obtained wavelength distribution and resolution results are shown in Figure 6. It can be seen that the changing trend of the overall spectral resolution of the system maintains the same trend as the spot radius data in Figure 6.

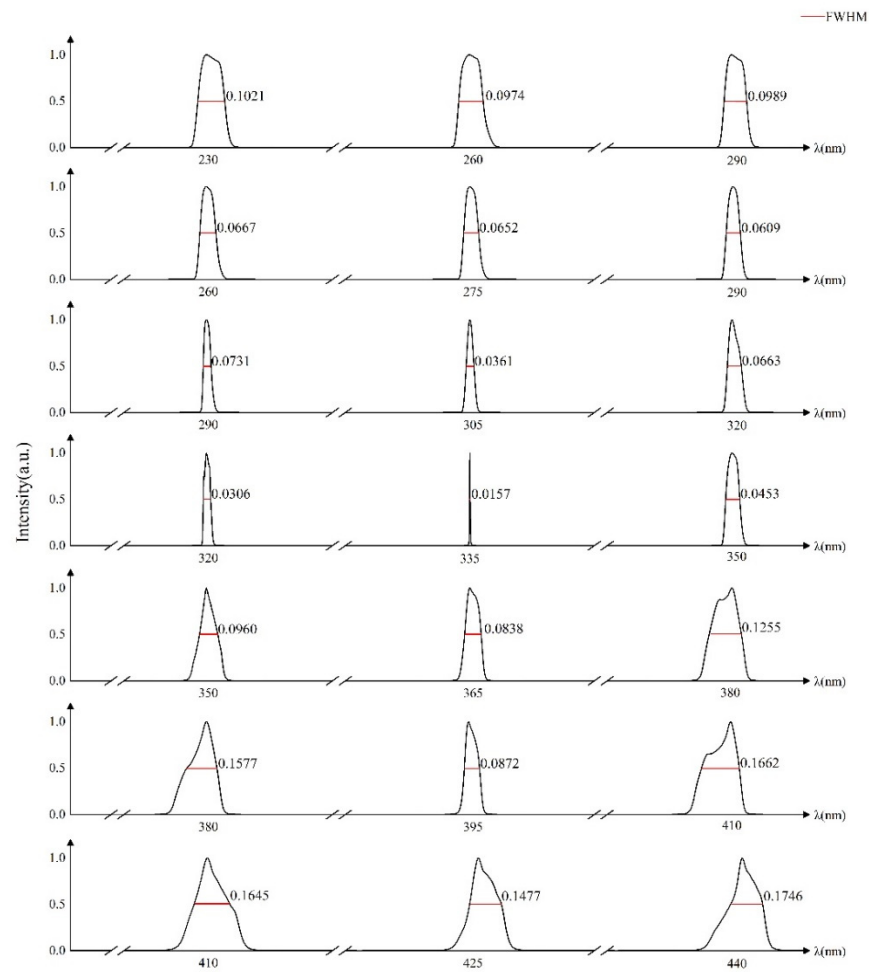


Figure 6. Curve of convolution of $f_S(x_s), f_{LSF}, f_D(x_d)$ at various wavelengths in the seven windows.

4. Discussion

Based on the purpose of stacking gratings on the sagittal plane in the C-T structure to improve the resolution, the gratings were divided and stacked on the sagittal plane in the traditional Paschen–Runge direct-reading spectrometer in this paper. It can be seen from the above experimental results that the overall size of the spectrometer was greatly reduced on the premise that the resolution met the requirements.

According to the comprehensive comparison between Figures 5 and 6, the spot size and resolution trends of different gratings are basically consistent. After our analysis, the possible reasons for the asymmetry of the resolution distribution in Figure 6 are as follows: (1) the main factors affecting the resolution are the spherical aberration and meridional coma caused by the off-axis angle of the concave grating; (2) according to the relationship between wavelength and resolution, $d = \lambda/2n\sin\theta$, when the incident angle is constant, the wavelength is proportional to the distance between the smallest two points that can be identified; (3) in order to make the simulation results closer to the real situation, this paper uses the LSF, slit function, and detector function convolved for resolution evaluation. To sum up, the inconsistent change trend of the wavelength resolution on the symmetrical grating is caused by the comprehensive influence of multiple factors such as wavelength, aberration, and resolution calculation method. In the future, we will conduct further in-depth research on this. At the same time, we believe that this improved spectrometer structure may have some reference value for optical coherence tomography [18–21]. To further increase the band range or improve the spectral resolution, it can be achieved by increasing the number of gratings on the sagittal plane or reducing the corresponding spectral range of each grating.

5. Conclusions

In this study, we proposed an integrated Paschen–Runge direct-reading spectrometer structure that utilizes seven concave gratings to simultaneously map spectra onto an area array detector. Using this method, we designed a spectrometer that operates in the 230–440 nm wavelength band. The performance of the optical system is evaluated by using the Y-spot radius and spectral resolution, respectively. The spectral resolution of the center wavelength corresponding to the seven grating windows of 230–260 nm, 260–290 nm, 290–320 nm, 320–350 nm, 350–380 nm, 380–410 nm, and 410–440 nm can reach 0.0974 nm, 0.0652 nm, 0.0361 nm, 0.0157 nm, 0.0838 nm, 0.0872 nm, and 0.1471 nm. The whole system has no moving mechanical parts, which increases the stability and reliability of the system. Using an area array detector to simultaneously receive the spectral signals of seven gratings increases the spectral consistency. We plan to build such a device in future research. Compared with the traditional Paschen–Runge structure, the optical system is smaller in volume and more compact in structure, which has a higher profit margin and good field detection prospects.

Author Contributions: Conceptualization, G.X.; validation, W.S. and Y.L.; visualization, L.G.; writing—review and editing, Z.F.; methodology and writing—original draft prep, L.Z. All authors have read and agreed to the published version of the manuscript.

Funding: This research received no external funding.

Conflicts of Interest: The authors declare no conflict of interest.

References

1. He, P.; Yuan, Y.; Lv, Q.; Li, B. Method for evaluating spectral resolution based on a single-lens spectrometer. *Appl. Opt.* **2021**, *60*, 7834–7843. [[CrossRef](#)] [[PubMed](#)]
2. Papp, Á.; Kiechle, M.; Mendisch, S.; Ahrens, V.; Sahin, L.; Seitner, L.; Porod, W.; Csaba, G.; Becherer, M. Experimental demonstration of a concave grating for spin waves in the Rowland arrangement. *Sci. Rep.* **2021**, *11*, 14239. [[CrossRef](#)] [[PubMed](#)]
3. Xiao, X.; Wang, Y.; Zhang, C.; Yang, X. Simultaneous Determination of Silver, Boron and Tin in Carbonate Minerals by Alternating Current-Arc Optoelectronic Direct Reading-Emission Spectrometry. *Rock Miner. Anal.* **2020**, *39*, 699–708.
4. Labusov, V.A.; Boldova, S.S.; Selunin, D.O.; Semenov, Z.V.; Vashchenko, P.V.; Babin, S.A. High-resolution continuum-source electrothermal atomic absorption spectrometer for simultaneous multi-element determination in the spectral range of 190–780 nm. *J. Anal. At. Spectrom.* **2019**, *34*, 1005–1010. [[CrossRef](#)]
5. Ramazanov, A.N.; Kostrin, D.K. Modeling of the optical schemes of small-sized spectrometers. *J. Phys. Conf. Ser.* **2018**, *1135*, 012062. [[CrossRef](#)]
6. Zeng, Q.; Sirven, J.B.; Gabriel, J.C.P.; Tay, C.Y.; Lee, J.M. Laser induced breakdown spectroscopy for plastic analysis. *TrAC Trends Anal. Chem.* **2018**, *140*, 116280. [[CrossRef](#)]
7. Chen, Y.; Sun, B.; Han, T.; Kong, Y.; Xu, C.; Zhou, P.; Li, X.; Wang, S.; Zheng, Y.; Chen, L. Densely folded spectral images of a CCD spectrometer working in the full 200–1000 nm wavelength range with high resolution. *Opt. Express* **2005**, *13*, 10049–10054. [[CrossRef](#)] [[PubMed](#)]
8. Xue, Q.; Lu, F.; Duan, M.; Zheng, Y.; Wang, X.; Cao, D.; Lin, G.; Tian, J. Optical design of double-grating and double wave band spectrometers using a common CCD. *Appl. Opt.* **2018**, *57*, 6823–6830. [[CrossRef](#)] [[PubMed](#)]
9. Fu, Y.; Wang, H.; Jia, X.; Ming, J.; Zheng, W.; Jin, N.; Wang, X. The optical system design of broadband infrared imaging spectrometer. In *Infrared, Millimeter-Wave, and Terahertz Technologies VII*; International Society for Optics and Photonics: Bellingham, WA, USA, 2020; Volume 11559.
10. Zeng, C.; Han, Y.; Liu, B.; Sun, P.; Li, X.; Chen, P. Optical design of a high-resolution spectrometer with a wide field of view. *Opt. Lasers Eng.* **2021**, *140*, 106547. [[CrossRef](#)]
11. Zhang, Y.; Gai, Y.; Yang, H.; Zhang, Y.; Huang, Z.; Jin, G. Broadband snapshot spectrometer based on spliced spectra. *Opt. Commun.* **2018**, *427*, 226–230. [[CrossRef](#)]
12. Jiang, A.; Zang, K.; Tu, H.; Chen, J.; Lu, W.; Yoshie, O.; Wang, X.; Xiang, X.; Lee, Y.; Chen, B.; et al. Ultrahigh-resolution spectrometer based on 19 integrated gratings. *Sci. Rep.* **2019**, *9*, 10211. [[CrossRef](#)] [[PubMed](#)]
13. Tu, H.; Jiang, A.; Chen, J.; Lu, W.; Zang, K.N.; Tang, H.-Q.; Yoshie, O.; Xiang, X.; Lee, Y.; Zhao, H.; et al. A coma-free super-high resolution optical spectrometer using 44 high dispersion sub-gratings. *Sci. Rep.* **2021**, *11*, 1093. [[CrossRef](#)] [[PubMed](#)]
14. Astronomical & Scientific Camera Scientific Cameras. Available online: <https://www.qhyccd.com/scientific-camera-qhy4040-pro/> (accessed on 27 October 2022).
15. Reimers, J.; Rolland, J.P. Spectral full-field displays for spectrometers. In *International Optical Design Conference*; Optical Society of America: Washington, DC, USA, 2014.

16. Shi, W.; Gao, L.; Zhang, L.; Feng, Z.; Fang, F.; Xia, G. The Evaluation of Spectral Resolution in the Optical Design of a Czerny-Turner Spectrometer. *Photonics* **2022**, *9*, 678. [[CrossRef](#)]
17. Lee, K.-S.; Thompson, K.P.; Rolland, J.P. Broadband astigmatism-corrected Czerny–Turner spectrometer. *Opt. Express* **2010**, *18*, 23378–23384. [[CrossRef](#)] [[PubMed](#)]
18. Ratheesh, K.M.; Seah, L.K.; Murukeshan, V.M. Spectral phase-based automatic calibration scheme for swept source-based optical coherence tomography systems. *Phys. Med. Biol.* **2016**, *61*, 7652. [[CrossRef](#)] [[PubMed](#)]
19. Meleppat, R.K.; Fortenbach, C.R.; Jian, Y.; Wagner, K.; Modjtahedi, B.S.; Motta, M.J.; Motta, M.J.; Ramamurthy, D.L.; Schwab, I.R.; Zawadzki, R.J. In Vivo Imaging of Retinal and Choroidal Morphology and Vascular Plexuses of Vertebrates Using Swept-Source Optical Coherence Tomography. *Transl. Vis. Sci. Technol.* **2022**, *11*, 11. [[CrossRef](#)] [[PubMed](#)]
20. Everett, M.; Magazzeni, S.; Schmoll, T.; Kempe, M. Optical coherence tomography: From technology to applications in ophthalmology. *Transl. Biophotonics* **2021**, *3*, e202000012. [[CrossRef](#)]
21. Kolokoltsev, O.; Gómez-Arista, I.; Treviño-Palacios, C.G.; Qureshi, N.; Mejia-Urriarte, E.V. Swept Source OCT beyond the Coherence Length Limit. *IEEE J. Sel. Top. Quantum Electron.* **2016**, *22*, 222–227. [[CrossRef](#)]